ARTICLES

Investigation of Interligand Electron Transfer in Polypyridyl Complexes of Os(II) Using Femtosecond Polarization Anisotropy Methods: Examination of $Os(bpy)_3^{2+}$ and $Os(bpy)_2(mab)^{2+}$

George B. Shaw, Carter L. Brown, and John M. Papanikolas*

Department of Chemistry, Venable and Kenan Laboratories, The University of North Carolina at Chapel Hill, Chapel Hill, North Carolina 27599-3290

Received: July 30, 2001; In Final Form: November 5, 2001

Femtosecond pump−probe polarization anisotropy measurements are used to investigate the interligand electron transfer (ILET) dynamics in two polypyridyl Os(II) complexes following photoexcitation to a metal-to-ligand charge transfer (MLCT) state. The two complexes studied are $Os(bpy)_3^{2+}$ (bpy = 2,2′-bipyridine) and a mixed-ligand analogue, $Os(bpy)_2(mab)^{2+}$, where *mab* is a mono-amide functionalized bipyridine ligand. In acetonitrile, the *bpy* → *bpy* ILET time is 8.7 ps in $Os(bpy)_3^{2+}$ and the *bpy* → *mab* ILET is 1.5 ps in $Os(bpy)_2(mab)^{2+}$. A solvent dependence study reveals that the ligand−ligand electron-transfer time (in both complexes) scales with the reorganization time of the solvent, suggesting that ILET in these complexes occurs in the adiabatic limit. An analysis of the anisotropy amplitudes for the excited-state absorption in $Os(bpy)_3^{2+}$ may provide evidence for the formation of a delocalized (or partially delocalized) excited state produced by optical excitation.

I. Introduction

The interest in the excited-state properties of Ru(II) and Os(II) polypyridyl coordination complexes (Figure 1) is motivated largely by their potential for use in solar energy conversion applications. To this end, the spectroscopy of these complexes has been widely investigated, and from this work has emerged a basic understanding of the excited-state properties of $Ru(bpy)_3^{2+}$, $Os(bpy)_3^{2+}$ (bpy = 2,2′-bipyridine), and their simple analogues.[1−11] The lowest energy excited states are metal-to-ligand charge-transfer (MLCT) in nature. MLCT excitation is followed by efficient intersystem crossing (ISC) to the triplet manifold. It is fairly well established that in polar solvents the electron distribution in the ^{3}MLCT state is localized by the solvent (at least at long times after photoexcitation) on a single bipyridine ligand,[6,7] and thus $[M^{III}(bpy)_2(bpy•−)]^{2+}$ is a qualitatively accurate description of the *equilibrated* excited state. While the nature of the $Ru(bpy)_3^{2+}$ and $Os(bpy)_3^{2+}$ excited states at long times after photoexcitation are generally agreed upon, many questions regarding evolution on faster time scales still persist.

In recent years, several accounts describing ultrafast experiments on $Ru(bpy)_3^{2+}$ and other homoleptic complexes have appeared in the literature.[12−14] By and large, these indicate the presence of rich excited-state relaxation phenomena taking place on the femtosecond time scale. For instance, transient absorption studies on $Ru(bpy)_3^{2+}$ suggest that relaxation to the triplet manifold occurs within a couple hundred femtoseconds after photoexcitation,[12] implying that ISC occurs in concert with other spin-allowed relaxation processes such as solvent reorganization and intramolecular vibrational redistribution (IVR). Even after relaxation into the lowest excited state has occurred, the wave function is not static, and on longer time scales the photoexcited electron can incoherently hop from one ligand to another in what amounts to an interligand electron transfer (ILET) process.

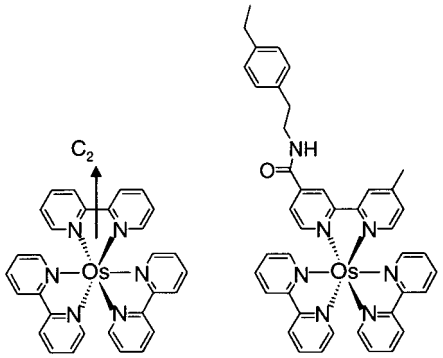

Figure 1. Chemical structures of the two Os(II) complexes discussed in this work. Os−BPY and Os−MAB refer to $Os(bpy)_3^{2+}$ and $Os(bpy)_2(mab)^{2+}$, respectively. In this notation, *bpy* and *mab* correspond to the bipyridine and mono-amide substituted bipyridine ligands, respectively. The *mab* ligand lies about 700 cm^{-1} lower in energy than *bpy*. The arrow in the Os−BPY diagram denotes one of the three C_2 symmetry axes.

ILET has received considerable attention in a variety of transition metal compounds.[15−24] We have explored this electron-transfer process in two polypyridyl Os(II) complexes using femtosecond pump−probe polarization spectroscopy. The molecular systems of interest are Os−BPY (BPY ≡ $(bpy)_3^{2+}$) and Os−MAB (MAB ≡ $(bpy)_2(mab)^{2+}$); their chemical structures

* To whom correspondence should be addressed. E-mail: John_Papanikolas@unc.edu.

10.1021/jp012924u CCC: $22.00
Published on Web 02/02/2002

are shown in Figure 1. The Kelley group[15−18] has investigated ILET in Ru−BPY and Os−BPY, also using polarization anisotropy methods. However, the enhanced time resolution of our apparatus (500 fs versus 10 ps) has yielded observations that are qualitatively inconsistent with theirs. Specifically, we measure the *bpy* → *bpy* ILET time in acetonitrile to be about 15 times faster than that reported by Kelley,[15] and through variation of the solvent we conclude that ILET takes place in the (strongly coupled) adiabatic limit.

The experiments described in this paper go beyond the symmetric Os−BPY complex and also describe observations made on a mixed-ligand complex, Os−MAB. Mixed-ligand complexes are quite common, and a large number have been synthesized. In part, this interest stems from their use as building blocks in larger arrays, where ligands with different substituents are needed to connect molecular subunits (see refs 25−27 for examples). The mixed-ligand complex used here is part of a macromolecular assembly that is currently under investigation in our laboratory for its light harvesting capability.[28] The Os−MAB complex is relatively simple when compared to the vast array of mixed-ligand complexes in existence, and thus it also serves as a model system for investigating the excited-state relaxation phenomena in a large number of complexes.

One consequence of this ligand asymmetry is that it affects the energies of the MLCT excited states. Because different ligands have different affinities for the excited electron, the MLCT states associated with different ligands have different energies. In this particular case, the electron withdrawing nature of the amide substituent allows for a larger delocalization of the π^* orbitals, and this stabilizes the *mab* MLCT state relative to the MLCT state associated with the unfunctionalized *bpy* ligand. This state ordering has been confirmed by transient infrared experiments[29] (on the ruthenium analog) that show the photoexcited electron on the *mab* ligand at long times after photoexcitation. The difference in energy between the two ligands has been established by electrochemical methods[30] to be approximately 700 cm^{-1}. Thus, there is a modest driving force for electron transfer that is not present in the Os−BPY complex, and as expected this results in faster ILET in the mixed-ligand species.

An important aspect of the discussion of the excited states is whether photoexcitation produces a localized excited state, or creates a delocalized state that then localizes due to environmental (inner- or outer-sphere) reorganization. The crucial issue is the magnitude of the ligand−ligand coupling in comparison to the nanoheterogeneity of the environment at the instant of photon absorption. The experimental evidence speaking to this point is mixed. In the past two decades there have been a variety of arguments both in favor of localized[31−35] and delocalized[14,36−40] excited states on the electronic time scale. Most of these experiments focused on the Ru−BPY complex. However, because the ruthenium and osmium analogues have different ligand−ligand couplings, the degree of delocalization in the initially prepared excited states may be quite different for Ru−BPY and Os−BPY. And so while the issues may be the same in the two complexes, the outcome may not.

Our experiments may speak to the nature of the excited-state charge distribution at the instant of photon absorption. One possible interpretation of the polarization anisotropy data presented in this paper is that the excited states (produced by excitation at the red-edge of the triplet absorption band) are partially delocalized over two or more of the ligands. In all likelihood this is a manifestation of an inhomogeneous excitation process arising from the distribution of local solvent environments at the instant of photon absorption. The observed anisotropy would then be an average over an excited-state ensemble that contains both localized and delocalized constituents. Our data is consistent with a ligand−ligand coupling that is large enough to yield adiabatic electron-transfer behavior, yet at the same time is smaller than (or comparable to) the degree of solvent inhomogeneity that is present when the complex is excited.

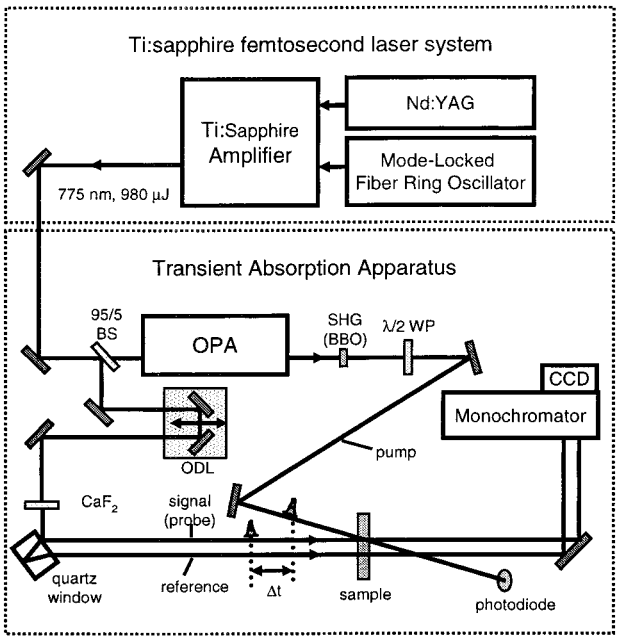

Figure 2. Schematic diagram of the femtosecond laser system and transient absorption apparatus used in this work.

II. Experimental Description

A schematic diagram of the laser system and the transient absorption apparatus is shown in Figure 2. The transient absorption spectrometer is based on a commercially available ultrafast laser system (Clark CPA-2001), consisting of an erbium-doped fiber ring oscillator and a chirped pulse Ti:sapphire regenerative amplifier that is pumped by a frequency-doubled, mode-locked, Q-switched Nd:YAG laser. The amplifier produces 120 fs laser pulses at 775 nm at 1 kHz with pulse energies of approximately 950 μJ/pulse. The amplified output is split into two beams by an uncoated glass window.

The larger, transmitted fraction (96%) pumps an optical parametric amplifier (OPA), which generates tunable femtosecond laser pulses. For the experiments described here, the output of the OPA is tuned to about 1400 nm and is frequency doubled to 700 nm to produce pulses with energies of about 10 μJ/pulse. This is the pump beam used to excite the osmium complexes in the transient absorption experiment. It is focused with a 30 cm lens to a spot size of $\approx$800 μm at the sample yielding a photon flux of approximately 10^{15} photons/cm^2. After passing through the sample, the pump beam is then directed into a photodiode for normalization of the transient absorption signal to changes in laser power.

The weak (4%) reflection from the front surface of the uncoated optic is used to generate the probe beam. This beam is directed into a computer-controlled translation stage that is used to vary the optical delay between pump and probe pulses. The resolution of the translation stage is 1 μm. After passing through the delay stage, it is focused with a 150 mm focal length

lens into a 6 mm thick CaF_2 window to generate a white light continuum, which is then collimated with an 80 mm focal length achromatic lens. Calcium flouride is used as the medium because the continuum it generates extends further into the UV (approximately down to 350 nm) than other substances, such as sapphire. The white light is split into two weaker beams of nearly equal intensity by taking the reflections off the front and rear surfaces of a 2.5 cm thick quartz window. The front surface reflection, denoted the signal beam, is used for the probe pulse. The rear surface reflection is used as the reference beam in the transient absorption measurement. The signal and reference beams are focused by 300 mm focal length fused silica lenses to a spot size of $\sim$150 μm at the sample. While both beams are directed through the sample, only the signal is spatially overlapped with the pump beam. The noncollinear approach of the pump and probe (signal) beams has an angle of approximately 2.5°. The signal and reference beams are simultaneously directed into a 0.27 m monochromator, dispersed with a 1200 line/mm holographic grating, and detected with a two-dimensional 1028 $\times$ 256 pixel liquid nitrogen cooled CCD array. This apparatus is capable of measuring a 77 nm segment of the transient absorption spectrum centered anywhere between 350 and 1000 nm with a sensitivity of better than 1 mOD.

The excited-state dynamics are followed through the evolution of the transient absorption spectra obtained at a series of pump−probe delay times. A typical data collection session consists of measuring transient absorption spectra at a series of 96 different pump−probe delay positions. First, the transient absorption spectrum at a given delay is measured. The intensity of the signal and reference beams are integrated during an 800 ms exposure of the CCD array and then used to calculate the excited-state/ground-state differential absorption (ΔA) spectrum. Ten exposures of the CCD camera are performed and the spectra from each are averaged together before moving on to the next pump−probe delay position. The entire set of pump−probe delay positions is repeated at least three times and the spectra obtained at like delays are averaged together. In some cases, the final spectrum represents a compilation of several different data collection sessions. Thus, each transient absorption spectrum represents an average over at least 24 000 (and in some instances as many as 150 000) laser pulses.

The frequency chirp in the while light continuum is characterized using the optical Kerr response of liquid CCl_4 to an intense laser field in a polarization gating geometry. The bottom pane in Figure 3 shows a contour plot of the Kerr signal as a function of pump−probe delay and probe wavelength. As the delay is increased the dominant frequency shifts to the red. This is a direct measure of the chirp in the white light pulse over the spectral range of interest. Between 360 and 420 nm (the spectral region of interest) the frequency chirp is approximately 2 ps. A horizontal slice through this surface is the cross-correlation at a specified probe wavelength. Several are shown in the top panel of Figure 3. Each has a fwhm of approximately 550 fs, which is about a factor of 2 greater than the pulse width of the laser. The primary source of this temporal broadening is a group velocity mismatch between the 700 nm pump beam and the 380 nm portion of the probe beam. This causes the pump and the probe pulses to travel at different speeds through the sample. By comparison, cross correlations with a portion of the continuum nearer to 600 nm are approximately 180 fs, which is closer to the durations of the individual pulses.

Both of the osmium complexes, $[Os(bpy)_3](PF_6)_2$ and $[Os(bpy)_2(mab)](PF_6)_2$, denoted Os−BPY and Os−MAB, respectively, were obtained as gifts from T. J. Meyer and used without further purification. The chloride salts of these compounds were used in experiments where ethylene glycol was the solvent. All of the solvents were spectral grade, and the acetonitrile was distilled over calcium hydride prior to use. The concentrations of all the samples used were adjusted to yield an optical density of approximately 0.25 at 450 nm in a 2 mm path length cell. All experiments were performed at room temperature.

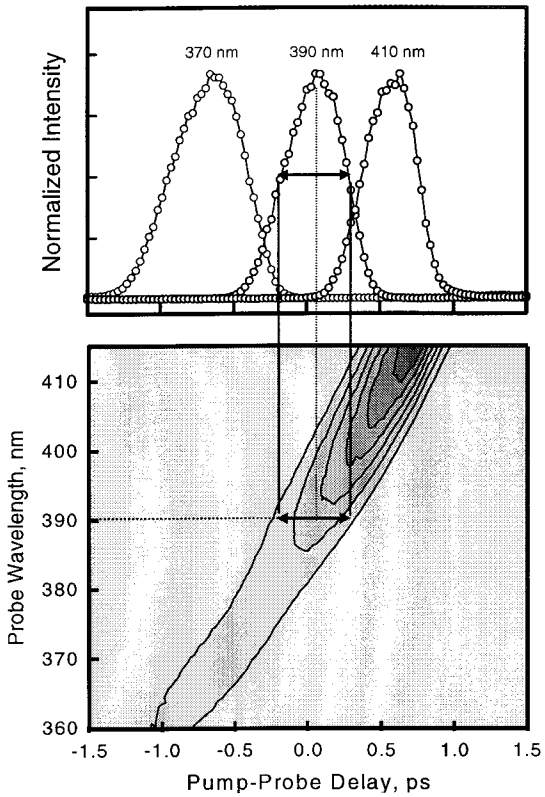

Figure 3. Bottom panel shows the intensity of the optical Kerr signal as a function of pump−probe delay and probe wavelength. The decrease in Kerr signal at the blue edge of the probe spectrum is a consequence of the lower intensity of the white light in that spectral region. The upper panel shows three time slices through this surface at different probe wavelengths. Each slice is normalized to the same intensity as the others and represents the cross correlation at the probe wavelength indicated in the figure. The fwhm of the cross correlation is $\approx$550 fs, which is broadened with respect to the laser pulse width due to group velocity mismatch between the pump and the probe pulses.

III. Results and Discussion

A comparison of the ground-state absorption spectra for Os−BPY and Os−MAB is shown in Figure 4. The primary difference between the two spectra is the presence of a slight red shift in the Os−MAB absorption features, which is consistent with a lower energy, *mab*-based MLCT state. Aside from this slight shift, the spectra are qualitatively similar; each shows an intense absorption band centered at about 450 nm and a weaker band that extends from approximately 520 nm to 700 nm. Both bands correspond to MLCT excitation. Photoexcitation within the stronger absorption feature promotes the complex to a singlet MLCT state. Afterward, the system undergoes efficient intersystem crossing to a low-lying triplet state.[41] Recent ultrafast experiments on Ru−BPY indicate that this takes place within a few hundred femtoseconds.[12] The analogous process in Os−BPY has not been fully characterized, but preliminary work in our laboratory suggests that the time scale for ISC in this complex may also be quite short.

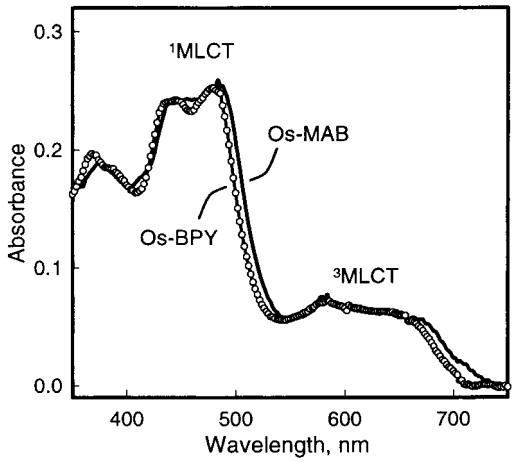

Figure 4. Ground-state absorption spectra of Os−BPY (points + line) and Os−MAB (line only) in room-temperature acetonitrile.

Photoexcitation within the weaker absorption feature corresponds to the direct population of the triplet state. There are, in fact, several ^{3}MLCT states associated with each ligand.[42−44] The lowest three states are primarily triplet in character, and lie within a hundred wavenumbers of each other. The fourth state, while still commonly described as a triplet, has a substantial amount of singlet character and resides about 300−600 cm^{-1} higher in energy.

We have performed experiments at both singlet and triplet excitation wavelengths. This paper focuses on excitation at the red edge of the triplet absorption band. For all of the experiments presented here, the Os−BPY and Os−MAB complexes were excited at 693 and 700 nm, respectively. By limiting excitation to the red edge of the triplet absorption, we promote the complex to the lowest energy excited-state accessible by optical excitation. This circumvents the singlet−triplet relaxation pathway and reduces the number of processes that contribute to the transient signals, thus simplifying the interpretation of the time-resolved data.

A. Solvated Electronic Structure. The Os−BPY complex has D_3 symmetry, and as such the electronic states of the *isolated* molecule are identified with either A or E symmetry labels. This is the case at the instant of photoexcitation, and ignoring any inner sphere reorganization effects, at long times as well. For a *solvated* molecule, the situation is somewhat different. At long times after photoexcitation, the charge is trapped by the solvent on a single ligand, thus making these symmetry labels irrelevant. Still uncertain, however, is the extent to which they are relevant for describing the MLCT excited states at the instant of photoexcitation. What is clear is that the excited-state wave function of the complex depends as much upon the details of the solvent environment as its own molecular Hamiltonian. One is thus forced to confront the electronic structure of the *solvated* species.

For a symmetric molecule like Os−BPY, the degree of charge delocalization in the MLCT state is determined by the relative magnitudes of the electronic coupling between the bipyridine ligands and the electrostatic asymmetry presented by the molecular environment. The ligand orbitals for a molecule embedded in a symmetric environment (e.g., the isolated molecule) will be degenerate, and a weak electronic coupling is sufficient to achieve complete delocalization. The situation may be quite different for an osmium complex embedded in a polar solvent. The electrostatic asymmetry presented by the local environment will lift the degeneracy of the three ligands, and

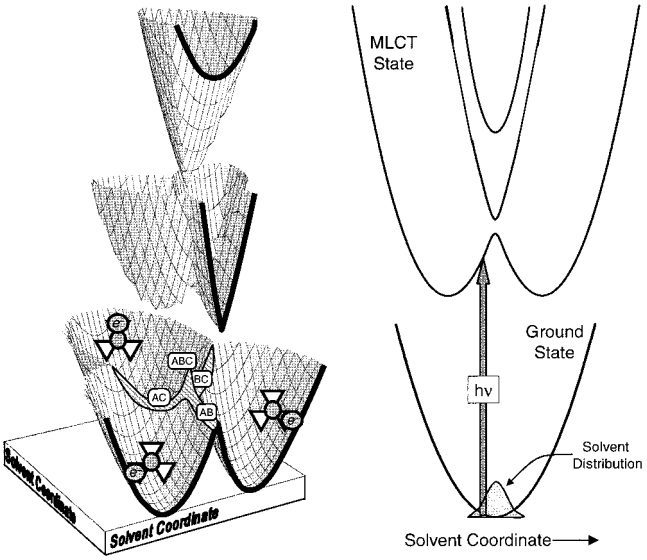

Figure 5. Illustration of the *solvated* MLCT excited-state potential surfaces for Os−BPY. The diagrams represent the extension of the classic Marcus−Hush diagram for electron transfer from a two-center to a three-center system. The diagram at the left is a 3-D representation of the three adiabatic surfaces, which are vertically offset for clarity. The minima in the lowest energy surface correspond to the localization of the charge by the solvent on a different bipyridine ligand. There is a diagram of this type associated with each MLCT excited state. The diagram at the right is a cross section through these surfaces, with the potential energy curves corresponding to the bold lines along the cut-out of the 3-D potential. The ground-state potential surface is displayed in the 2-D diagram, but is omitted from the 3-D picture.

if the asymmetry is large enough, the electronic states will have a localized charge distribution.

A schematic diagram of a potential surface illustrating these concepts is shown in Figure 5. This picture is a qualitative extension of the classic Marcus−Hush diagram from a two-center to a three-center system. The excited-state energies are displayed as a function of a two-dimensional solvent coordinate, which is necessary to describe a system with three sites for the location of the electron. As such, three diabatic surfaces are needed to describe Os−BPY, one for the localization of the electron on each of the three ligands. In keeping with Marcus−Hush theory, these diabatic states are represented by parabolic surfaces placed at the corners of an equilateral triangle within this two-dimensional solvent plane. Electronic mixing between the ligands leads to the formation of an avoided crossing at the intersections between the diabatic states, resulting in the three adiabatic surfaces depicted in Figure 5. For clarity, these surfaces are vertically offset from each other in the figure.

The lowest energy adiabatic surface has three distinct minima, each corresponding to the localization of the charge on a different bipyridine moiety. In the context of this diagram, ILET corresponds to movement from one minimum to another. Not all points on this surface correspond to localized excited states, however. Along the ridge denoted AB (which marks the intersection between the diabatic surfaces of A and B) the solvent brings ligand A into resonance with ligand B (but not C). For points along this boundary, the excited-state wave function has C_2 symmetry. There are two other two-center resonance seams, marked AC and BC. The point marked ABC corresponds to the totally symmetric solvent configuration that simultaneously brings all three ligands into resonance. This is the only point on the excited-state potential energy surface in which it is appropriate to discuss the electronic structure of Os−BPY in the context of the D_3 point group.

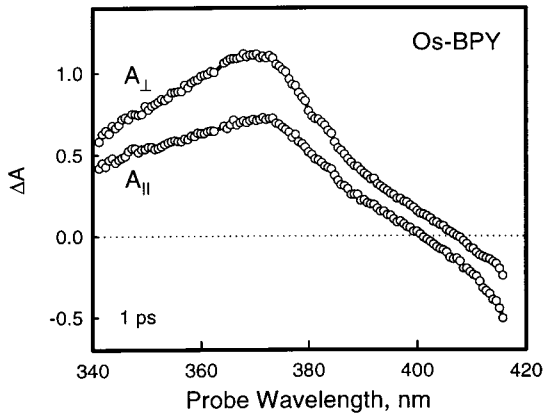

Figure 6. Transient absorption spectra observed 1 ps after photoexcitation of Os−BPY in room-temperature acetonitrile. The two spectra were obtained with pump and probe polarization vectors set to be parallel ($A_{||}$) or perpendicular ($A_\perp$).

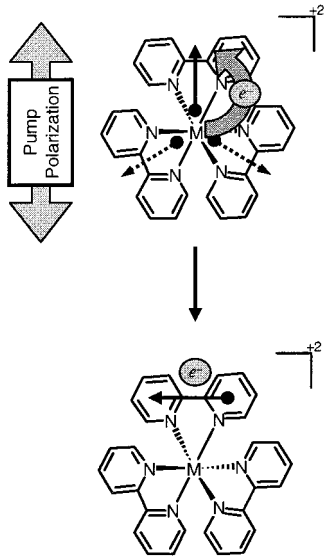

Figure 7. Illustration of the photoselection process in Os−BPY for a vertically polarized excitation laser. Arrows placed within the chemical structure depict the direction of the transition dipoles for MLCT excitation (top) and probe transition dipole (bottom). The excitation dipoles are depicted for the weak ligand−ligand coupling (i.e., localized excited-state) limit.

Strictly speaking, delocalized wave functions with C_2 or D_3 symmetry are only present for complexes that lie along one of the ridges, or at the central cusp point. This is blurred, to some extent, by the ligand−ligand coupling, and thus a region of delocalized excited states exists in the vicinity of the avoided crossings. This region is identified in the figure by the "outlined" area. Its size will depend on the magnitude of the coupling, and for a weak coupling, it will be relatively narrow. But, as the coupling increases more inhomogeneity in the solvent environment can be overcome, and the region corresponding to delocalized wave functions will broaden. It has been suggested[15,40] that the ligand−ligand coupling is about 2−20 cm^{-1}. The experiments presented in this paper suggest that this is too small, and indicate a somewhat larger value of several hundred wavenumbers.

The localized versus delocalized nature of the wave function is determined by the initial location of the system on this potential surface, which is linked to the configuration of the solvent when the photon is absorbed. Thus the relevant question is: what is the distribution of solvent configurations that surround the *ground-state* complex? The ground state has no dipole moment, and so the minimum of its potential surface, and the center of this distribution, is located directly below the central cusp point (ABC) of the excited-state potential. The excited-state ensemble will therefore be a superposition of both localized and delocalized excited states. The relative contribution of each is determined by the distribution of solvent configurations and the magnitude of the electronic coupling. It is also dependent upon the color of the excitation photon, as not every member of the ground-state ensemble will be excited at a given photon energy. At the red edge of the triplet absorption band there is a preferential excitation of the systems that lie in the wings of the distribution. This will tend to produce localized excited states, and generally speaking our data bear this out. But, in addition to this localized fraction, our data seem to suggest that a significant subset of the excited-state ensemble is initially delocalized. This would imply that there is a fairly broad region of the potential surface that corresponds to delocalized excited states, and is consistent with our finding of a large electronic coupling and rapid ILET. This is discussed in more detail in Section E.

B. Transient Absorption; General Considerations. The excited-state dynamics are followed using femtosecond transient absorption methods. Displayed in Figure 6 are transient absorption spectra observed for Os−BPY 1 ps after photoexcitation at 693 nm. Two spectra are shown—one obtained with the pump and probe polarizations parallel to each other, and the other perpendicular. Both have an intense absorption centered in the neighborhood of 370 nm that arises from a ligand-localized $\pi\pi^*$ transition on the bipyridine radical anion (bpy^-) fragment of the MLCT excited state.[45−49] The difference in magnitude between the two spectra results from a photoselection process, which is depicted schematically in Figure 7.

Photoexcitation with linearly polarized light preferentially excites those molecules whose absorption dipoles are aligned along the laser polarization vector. For Os−BPY, the low energy MLCT excitations are polarized in the plane containing the three C_2 axes, i.e., the axes that extend from the metal center and bisect the bipyridine ligands.[50] The orientation of the dipoles within this plane depends on the degree of localization in the excited-state wave function. If the excited states are localized, then the three ligands will be independent of each other. In this limit, the excitation can be regarded as a superposition of three separate transition dipoles, each directed along a C_2 symmetry axis. Photoexcitation with linearly polarized light will then promote an electron to the ligand that is most closely aligned along the laser polarization vector. The probe transition dipole is oriented along the long axis of the bipyridine ligand,[49] perpendicular to the excitation dipole. Thus, the greatest excited-state absorption is observed when the probe beam is polarized perpendicular to that of the pump beam, as is observed. The relative intensities of the parallel and perpendicular spectra are thus a measure of the anisotropy in the excited-state transition dipole distribution.

The parallel and perpendicular transient absorption spectra also carry information about the excited-state populations (as would be observed in a conventional flash photolysis experiment). The separation of the population and anisotropy contributions to the data is essential for the interpretation of the transient signals. Spectra collected at the so-called "magic angle" polarization contain only population information. These can either be obtained directly, by measuring transient spectra with the angle between the pump and probe polarizations set to 54.7°

(the magic angle), or constructed from the parallel and perpendicular data, i.e.,

$$A_{MA} = \frac{1}{3}(A_{||} + 2A_{\perp}) \quad (1)$$

The polarization anisotropy, $r(t)$, contains information regarding changes in the transition dipole direction, and is defined as:

$$r(t) = \frac{A_{||} - A_{\perp}}{A_{||} + 2A_{\perp}} \quad (2)$$

The polarization anisotropy will take on a definite value determined by the relative orientation of the pump and probe transition dipoles. For nondegenerate transitions the anisotropy at early delay times, $r(t = 0,\theta)$ is given by

$$r(t = 0,\theta) = \frac{1}{5}(3\cos^2\theta - 1) \quad (3)$$

where θ is the angle between the pump and probe excitations. In many polarization anisotropy measurements, the initial value for $r(t)$ must be between $+0.4$ and -0.2, with the limiting cases corresponding to parallel ($\theta = 0°$) and perpendicular ($\theta = 90°$) excitations, respectively. This is the case in time-resolved fluorescence measurements, for example. The situation in transient absorption spectroscopy is somewhat more complicated, and this is discussed in more detail in Section D.

Polarization anisotropy is the ideal means for studying ILET in transition metal complexes. In Os−BPY all three ligands are identical, and thus the transfer of the electron from one ligand to another will not give rise to changes in the shape or amplitude of the excited-state spectra. Thus the magic angle spectra cannot provide information about the ligand−ligand hopping process. This is not the case for polarization anisotropy. As the electron hops from one ligand to another, the direction of the $\pi\pi^*$ transition dipole changes, and this degrades the anisotropy. Thus, the decay in r(t) with time after photoexcitation provides a direct indicator of the ligand−ligand hopping.

The application of polarization anisotropy to the study of ILET hinges upon the ability of the optical excitation to create a *localized* charge distribution. If the coupling between the ligands is large enough to overcome the asymmetry in the solvent environment, the optically prepared excited state will be delocalized, and the direction of the transition dipoles for MLCT excitation will be ill defined. As a result, there will be no correlation between the polarization vector of the laser and the initial location of the photoexcited electron. In this limit, polarization anisotropy cannot be used to probe the ILET process.

C. Magic Angle. The "magic angle" spectra observed at 400 ps after photoexcitation are shown in Figure 8 for the two complexes. The absorption feature that dominates this spectral region arises from a ligand localized $\pi\pi^*$ transition.[45−49] For Os−BPY, this is a bpy^- absorption. For the mixed-ligand complex it is an excitation of the lowest energy ligand, which in this case is mab^-. A comparison of the limiting spectra indicates that the absorption of the mab^- ligand is red shifted relative to that of its bipyridine parent, which is qualitatively consistent with the more delocalized π-network in that ligand.

The time evolution of the Os−BPY and Os−MAB spectra is depicted in Figure 9, which show the transient absorption signal as a function of pump−probe delay at several different probe wavelengths. In our analysis of the transient absorption data we examined seven probe wavelengths dispersed across

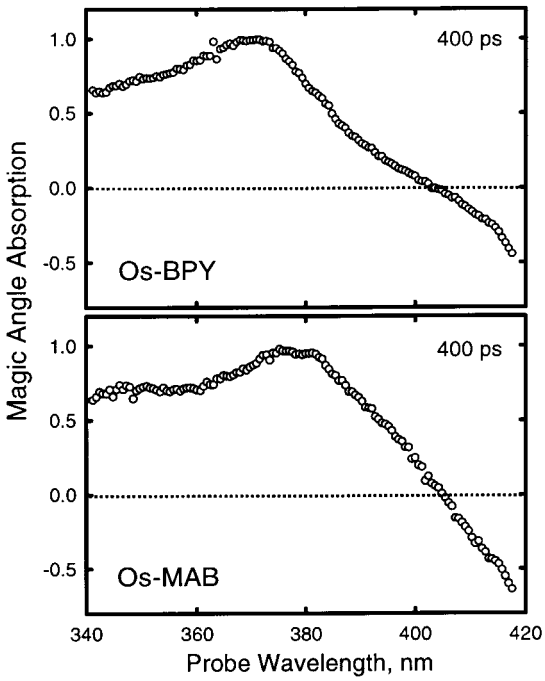

Figure 8. Magic angle spectra observed at 400 ps after photoexcitation of Os−BPY and Os−MAB. Os−BPY is excited at 693 nm and Os−MAB is excited at 700 nm. These are limiting spectra and reflect a ligand-localized $\pi\pi^*$ absorption on the lowest energy ligand. For Os−MAB this is the *mab* ligand.

this spectral region, although only three are shown for each complex. In both complexes there is a slight spectral reshaping that occurs in the first few picoseconds after photoexcitation. It is complete within 2−3 ps for Os−BPY and 10−15 ps for Os−MAB. In principle, this spectral evolution could stem from changes in either the ground-state bleach or excited-state absorption.

There are two possible contributions to spectral evolution of the bleach. The most obvious is the replenishment of the ground-state population, which would lead to an overall decrease in both the excited-state absorption and ground-state bleach contributions to the spectrum. This process can be ruled out because the excited state lifetimes of these osmium complexes are about 50 ns, and therefore, there is essentially no relaxation back to the ground state on the time scale of these experiments. The photoselective bleaching of a spectrally inhomogeneous ground-state population is another possible source. This is identical to the bleach evolution studied in transient hole burning experiments, which probe fluctuations in the solvent shell surrounding ground-state molecules. Recent ultrafast experiments[12] on Ru−BPY indicate that evolution in the bleach region of the spectrum (400−500 nm) is complete within 300 fs after photoexcitation. Since one would expect the time scale for solvent fluctuations surrounding a ground-state Ru−BPY complex to be similar to that for Os−BPY, this suggests that any bleach evolution that does occur is probably complete within a few hundred femtoseconds after photoexcitation. For this reason the observed spectral changes are attributed solely to changes in the excited-state absorption.

To quantify the changes at early delays, the magic angle absorption surface of each complex is fit to an exponential function of the form

$$A^{\lambda}_{MA}(t) = c^{\lambda}_1 \exp(-k_1 t) + c^{\lambda}_2 \exp(-k_2 t) + c^{\lambda}_{\infty} \quad (4)$$

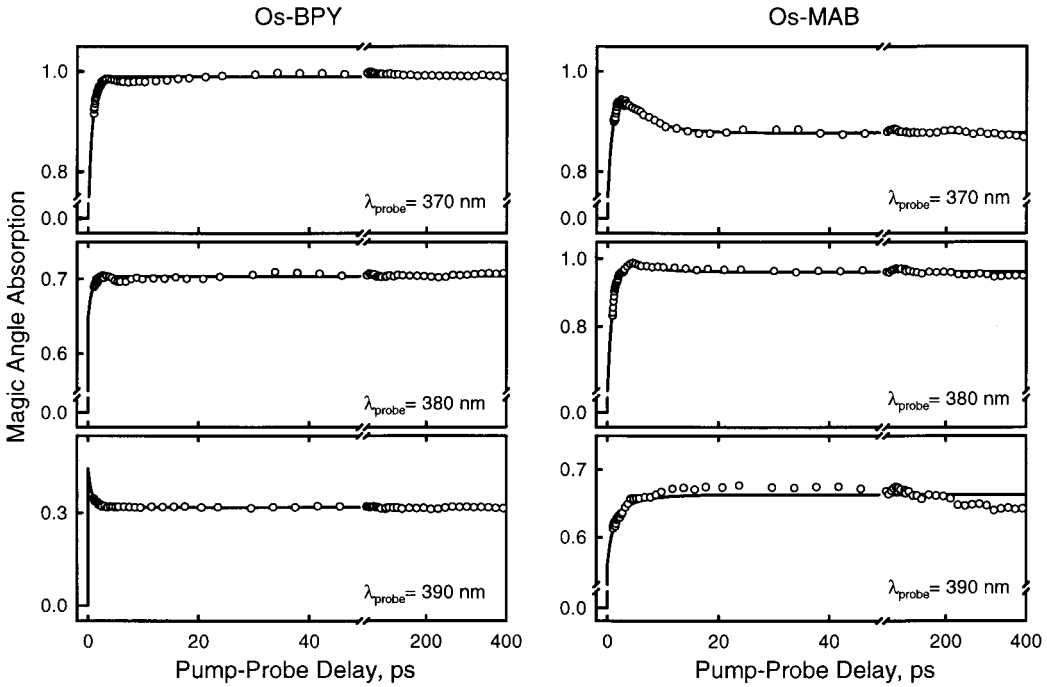

Figure 9. Transient absorption signal as a function of pump−probe delay for Os−BPY (left) and Os−MAB (right) in room-temperature CH_3CN. Transients at three probe wavelengths are shown for each complex; however, in our analysis of the data, seven such transients are utilized. A single exponential with a 0.75 ps time constant can describe all seven transients for Os−BPY. For the mixed ligand complex, a biexponential function with time constants of 1.0 and 4.5 ps are needed to obtain an adequate fit.

where λ refers to the probe wavelength, the rate constants (k_1 and k_2) are the same for λ's, and the amplitudes (c_1^λ, c_2^λ, and c_∞^λ) vary from one probe wavelength to another. The analysis involves the simultaneous fit of transients at seven different probe wavelengths.

The transient absorption surfaces of both complexes are well described by this functional form. The Os−BPY data can be fit using a single-exponential term with a 0.75 ps time constant. The spectral evolution in the mixed-ligand species is more complex, and two exponential terms (with 1 ps and 4−5 ps time constants) are needed. The solid lines in Figure 9 are the results of this fit. Displayed in Figure 10 are the coefficients that correspond to the growth (or decay) of the transient absorption signal, c_1^λ and c_2^λ. These are displayed such that a positive number reflects growth in the transient absorption signal. The fast decay component shows spectral changes that are qualitatively the same in both complexes. The similarities extend beyond just the fact that they evolve on similar time scales (0.75 ps vs 1.0 ps). In both cases there is a growth near the absorption maximum that is accompanied by a slight spectral narrowing. Rapid evolution in the transient spectra of polypyridyl complexes is not without precedence. McCusker and co-workers[12] have observed dramatic spectral changes in the first few hundred femtoseconds after the photoexcitation of Ru−BPY, which were attributed to single−triplet relaxation. The origin of the rapid growth in the Os−BPY and Os−MAB complexes is still not clear. It could arise from slight changes in the $\pi\pi^*$ absorption band that occur during relaxation through the low-lying triplet states and/or fast inertial reorganization of the solvent about the nascent charge distribution formed by MLCT excitation. Whatever the origin of this fast spectral reshaping, it appears to stem from a dynamical process that is common to both complexes.

The slow component is only present in the mixed-ligand complex, suggesting that its dynamical origin stems from the *mab* ligand. The coefficients associated with this kinetic component show growth at the absorption band's red edge and simultaneous decay at its blue edge, amounting to what is a red shift in the absorption band. The time constant for this

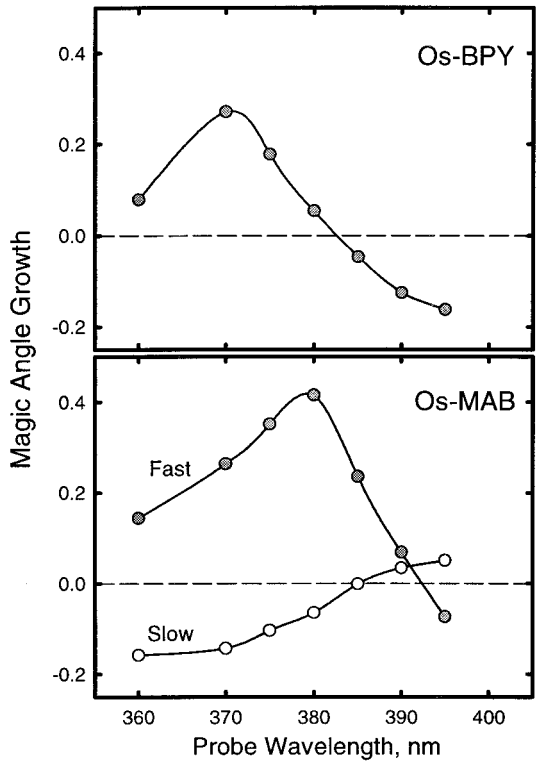

Figure 10. Amplitudes (c_1^λ and c_2^λ) obtained from nonlinear least-squares fit of magic angle spectral data to exponential functions. (Top panel) Results for Os−BPY, where only a single (0.75 ps) exponential function is needed. Thus, only a single amplitude (c_1^λ) is displayed. (Bottom panel) Results for Os−MAB. Two exponentials (1.0 and 4.5 ps) are needed to obtain an adequate fit for this complex. Filled and open circles represent amplitudes of fast and slow components, respectively. Positive numbers indicate growth of the transient absorption signal at that probe wavelength. Negative numbers indicate decay.

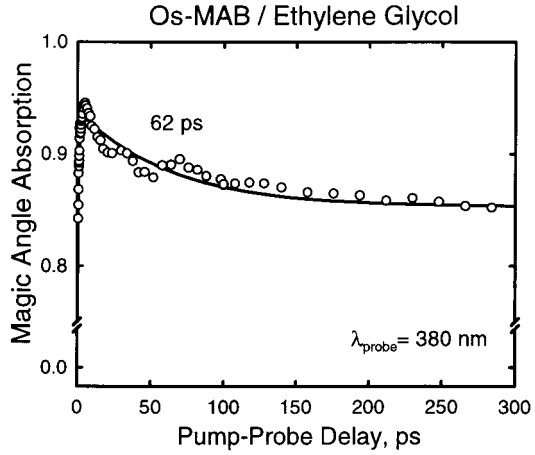

Figure 11. Transient absorption signal obtained for Os−MAB in room-temperature ethylene glycol. There is a rapid (0.7 ps) growth in the transient absorption signal at this probe wavelength followed by a slow (62 ps) decay. The time scale for the growth in ethylene glycol is similar to that observed in CH_3CN, but the decay is much slower. A rapid growth is also observed for Os−BPY in ethylene glycol (data not shown), but unlike Os−MAB there is no decay in the transient absorption signal at long delay times.

spectral shift depends on the reorganization time of the solvent. Shown in Figure 11 is the transient absorption signal at 380 nm for Os−MAB in room-temperature ethylene glycol. While the fast component in this solvent (0.7 ps) is similar to that observed in CH_3CN, the slow kinetic component (63 ps) is about 10 times longer. One possible origin for this slow component is intramolecular vibrational relaxation. While one would expect the relaxation time to be solvent dependent, the observation that the decay is almost 10 times faster in acetonitrile seems too large to attribute to vibrational relaxation. Another possibility is that it reflects the *bpy* → *mab* ILET process. However, this assignment is not consistent with the polarization anisotropy data discussed in Section D. A third possibility is that the red spectral shift arises from the solvation of the mab^- ligand *after* ILET occurs. The "diffusive" reorganization time of acetonitrile is 2−3 ps.[51] Ethylene glycol exhibits multiexponential solvation kinetics with diffusive reorganization times ranging from 4 to 284 ps.[51] The qualitative scaling of the spectral reshaping times with the diffusive reorganization times supports this assignment.

D. Polarization Anisotropy. Our discussion of the polarization anisotropy data is divided into three sections. In the first section we develop a framework in which to quantitatively analyze anisotropy data obtained in a transient absorption experiment. This discussion is motivated by anomalous anisotropy values observed at early pump−probe delay times. In the second section the anisotropy decays for Os−BPY and Os−MAB are discussed in the context of ILET. Based on solvent-dependence measurements, it is concluded that ILET occurs in a strongly coupled adiabatic limit. In the third section, the anisotropy amplitudes are analyzed taking into account the effects of the bleach. This analysis may speak to the nature of the excited state at the instant of photoexcitation and would seem to suggest the presence of a delocalized (or partially delocalized) wave function in a significant fraction of the excited-state ensemble.

1. Basic Framework. For most time-resolved spectroscopy methods, the magnitude of the polarization anisotropy lies in the range +0.4 to −0.2. The case is not always quite so simple for transient absorption spectroscopy. Figure 12 shows $r(t)$ for Os−BPY as a function of the probe wavelength at early pump−probe delays. Between 390 and 410 nm, $r(t)$ lies outside of the

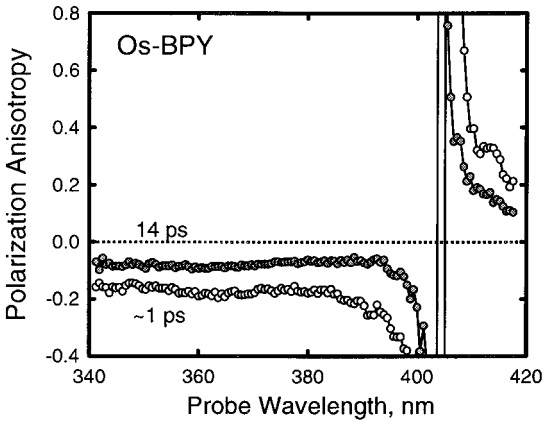

Figure 12. Polarization anisotropy, $r(t)$, as a function of the probe wavelength for Os−BPY in room-temperature CH_3CN. The open and filled circles are the anisotropy observed at 1 and 14 ps after photoexcitation, respectively.

normally expected range. A similar anisotropy spectrum is observed for the mixed ligand complex. There are two potential explanations for this behavior.

One possibility is that the anomalous $r(t)$ values arise from coherence effects. Indeed, a recent ultrafast experiment suggests that these are important in Ru−BPY,[14] especially within the first few hundred femtoseconds after photoexcitation. If coherence effects are the source, then this discontinuity in $r(t)$ should decay on a time scale commensurate with the lifetime of the coherence. This is not the case. The anisotropy spectrum at 14 ps after photoexcitation shows this same behavior. Since this is much longer than one might expect coherence to be maintained, it seems unlikely that it is the source of the anomalously large values observed here.

The more likely cause stems from the different contributions to the transient absorption signal itself. Differential absorption spectra are a superposition of both positive (absorption) and negative (bleach) going signals. Of course, stimulated emission can also contribute to the negative going signal, but that is not an issue in these experiments. When the positive and negative contributions nearly offset each other (i.e., are of similar magnitude) and have different polarization characteristics, the polarization anisotropy will lie outside the normally expected range dictated by eq 3. The origin of this can be seen by writing the parallel and perpendicular absorptions as

$$A_{\parallel}(t) = \alpha_{\parallel}^{T}(t) - \beta_{\parallel}^{T}(t) \tag{5a}$$

$$A_{\perp}(t) = \alpha_{\perp}^{T}(t) - \beta_{\perp}^{T}(t) \tag{5b}$$

where α^T and β^T refer to the *total* absorption and bleach contributions, respectively. (In this formalism, α and β are both positive quantities). The "magic angle" absorption is simply

$$A_{MA}(t) = \frac{1}{3}(\alpha^{T}(t) - \beta^{T}(t)) \tag{6}$$

where $\alpha^T = (\alpha_{\parallel}^T + 2\alpha_{\perp}^T)$ and $\beta^T = (\beta_{\parallel}^T + 2\beta_{\perp}^T)$. The polarization anisotropy measured in a transient absorption experiment is a weighted average of absorption and bleach anisotropies, $\langle r_\alpha(t)\rangle$ and $\langle r_\beta(t)\rangle$, and is given by

$$r(t) = \frac{\alpha^{T}}{\alpha^{T} - \beta^{T}}\langle r_{\alpha}(t)\rangle - \frac{\beta^{T}}{\alpha^{T} - \beta^{T}}\langle r_{\beta}(t)\rangle \tag{7}$$

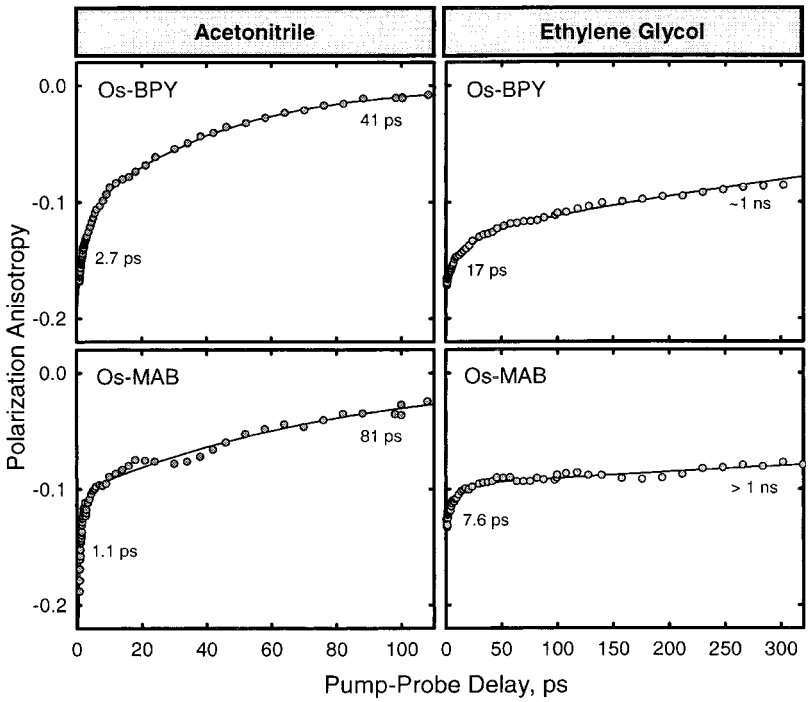

Figure 13. Decay in polarization anisotropy, $r(t)$, detected near the excited-state absorption maximum for Os−BPY and Os−MAB. The details for each panel are as follows: upper-right panel is Os−BPY in CH_3CN, upper-left is Os−BPY in ethylene glycol, lower-right is Os−BPY in CH_3CN, and lower-left is Os−MAB in ethylene glycol. Os−BPY and Os−MAB were excited at 693 and 700 nm, respectively. The decays are displayed for a 370 nm probe wavelength for Os−BPY and 380 nm for Os−MAB. All solvents were at room temperature.

If the absorption has contributions from multiple transitions, then $\langle r_a(t)\rangle$ is a weighted average,

$$\langle r_\alpha(t)\rangle = \sum_i \left(\frac{\alpha_i}{\alpha^T}\right) r_{\alpha,i}(t) \qquad (8)$$

where α_i represents the intensity of the individual transitions whose time-dependent anisotropies are given by $r_{\alpha,i}(t)$. There is a similar expression for the bleach anisotropy. When the bleach and absorption have different polarization characteristics (i.e., $\langle r_\alpha(t)\rangle \neq \langle r_\beta(t)\rangle$), $r(t)$ depends inversely on $(\alpha^T - \beta^T)$, and thus explains (at least qualitatively) why it diverges in the neighborhood of the transient absorption zero crossing. Other groups[14,52,53] have used similar expressions to explain anomalous anisotropy observations in transient absorption experiments.

Equation 7 provides a quantitative framework in which to discuss the anisotropy data. It shows that the observed anisotropy in a transient absorption experiment has contributions from not only the excited-state absorption anisotropy, but also the bleach anisotropy. In addition, through α^T and β^T it depends on the magnitude of the transient absorption signal. Because α^T and β^T could vary with pump−probe delay due to changes in excited-state populations, solvation dynamics, or intramolecular vibrational relaxation, their presence in eq 7 is a way for dynamical processes that *do not involve a change in transition dipole direction* to enter into the anisotropy decay. Thus, polarization anisotropy data collected in a transient absorption experiment must be interpreted with caution in order to avoid reaching erroneous conclusions.

2. Anisotropy Decay. Shown in Figure 13 are the anisotropy decays at 370 nm for Os−BPY and 380 nm for Os−MAB. The left-hand panels were obtained with acetonitrile as the solvent, and the right-hand panels are obtained when the complexes are dissolved in ethylene glycol. The individual points are the experimental data and solid lines are the result of a biexponential fit. All four transients show clear biphasic behavior; the time constants corresponding to the various kinetic components are indicated in the figure. In ethylene glycol, the decay times for the slow components are just estimates, since it is difficult to extract an exact time constant due to the limited pump−probe delay range over which the data were collected.

Kelley and co-workers[15−18] have performed similar polarization anisotropy measurements on both Ru−BPY and Os−BPY in a variety of polar solvents, including CH_3CN and ethylene glycol. The time constants for the slow components are consistent with the values reported by Kelley,[15] in both solvents. The slow component is attributed to rotational diffusion. This process is about a factor of 2 slower in Os−MAB than it is in Os−BPY, which is not surprising given the larger size of the *mab* ligand. When dissolved in ethylene glycol, the rotational diffusion times of both complexes increase, which is consistent with the higher viscosity of that solvent.

While the time constants for the slow components are in qualitative agreement with Kelley's, the decay times for the fast components are not. Kelley reports a 23 ps time constant in CH_3CN,[15] which is about 10 times slower than what we observe (2.7 ps). In ethylene glycol, the difference is less dramatic: 33 ps compared with 17 ps observed in our laboratory.[15] The origin of these discrepancies is unclear, but could be due to the use of a different probe wavelength (345 nm), or the slower time resolution of their instrument (10−15 ps).

There are several potential origins for the fast time component that must be considered. Ultimately we assign it to ILET in the MLCT excited state. However, before proceeding we present the other possibilities, and our arguments for dismissing them. According to eq 7, the observed anisotropy, $r(t)$, has contributions from the absorption and bleach anisotropies ($\langle r_\alpha(t)\rangle$ and $\langle r_\beta(t)\rangle$), and their relative amplitudes (α^T and β^T). In principle, any one of these could be responsible for the fast decay component. Since each can evolve on a different time scale, disentangling the different contributions to $r(t)$ will, generally speaking, be difficult. This task is simplified somewhat for Os−

BPY, where the magic angle signal (and hence α^T and β^T) does not have a 3 ps time component, in either solvent. This implies that the greatest contribution to the time dependence of $r(t)$ must come from $\langle r_\alpha(t)\rangle$ and/or $\langle r_\beta(t)\rangle$. We eliminate $\langle r_\beta(t)\rangle$, because it arises from rotational diffusion of the *unexcited complexes* in the sample, and therefore should only contribute to the slow component of the decay. The fast decay component must, therefore, stem from a dynamical process that takes place in the excited state.

We rule out relaxation through the manifold of low-lying triplet states as the source of this rapid decay. In order for changes in the electronic state to degrade the anisotropy, the transition dipole direction for the excited-state absorption would have to be different in each of the different states. It is unlikely that this is the case, however. The difference between the low-lying ^{3}MLCT states is determined primarily by the electronic configuration on the metal, not the bipyridine ligand. And since the $\pi\pi^*$ absorption is a ligand-localized transition, the direction of its transition dipole is expected to be the same for all of the MLCT states.

We attribute the fast decay component to ILET. This assignment is supported by two observations. The first is that the anisotropy decay times are consistent with the ligand energetics. As mentioned earlier, Os−MAB has a 700 cm^{-1} driving force for *bpy* → *mab* electron transfer, implying that the mixed-ligand complex should have a faster interligand hopping time than its symmetric counterpart, Os−BPY. This is, in fact, the case in both solvents. The second observation is that the decay time in each complex scales with the solvent reorganization time. When either complex is dissolved in ethylene glycol, its fast decay component is 6−7 times slower than it is in CH_3CN. This is generally the case for strongly coupled electron-transfer reactions, implying that the ILET process takes place in the adiabatic limit. This point is pursued further in Section E.

The connection between the observed decay time in $r(t)$ and the ILET time is relatively straightforward. For a totally symmetric complex like Os−BPY, the forward and backward electron-transfer rates are all identical. In this limit ILET rate constant is $^1/_3(k_{obs} - k_r)$, where k_{obs} is the observed anisotropy decay rate and k_r is the rate of decay due to rotational diffusion. Thus, the (2.7 ps)$^{-1}$ and (41 ps)$^{-1}$ decay rates observed in CH_3CN imply a *bpy* → *bpy* ILET time of 8.7 ps, which is about 15 times faster than the 130 ps time previously reported. In ethylene glycol the *bpy* → *bpy* ILET time is 52 ps. For the mixed ligand complex the forward and backward electron-transfer rates are not equal. In the limit that the *mab* → *bpy* electron transfer is slow compared to *bpy* → *bpy* and *bpy* → *mab* electron transfer, the ILET time for transfer to the lower energy *mab* ligand is estimated to be 1.5 ps in CH_3CN and 11 ps in ethylene glycol.

Recent evidence of ILET has been observed in two other mixed-ligand complexes, both of which support our notion of fast ligand−ligand electron transfer. Zewail and co-workers[23] report a 700 fs ILET time in dipyrido[3,2-*a*:2′-3′-*c*]phenazine (dppz) containing Ru(II) compound. Vlcek and co-workers[24] have also observed fast (≈8 ps) ILET in a mixed-ligand Re complex. The primary difference between these two compounds and Os−MAB is that their driving force for electron transfer exceeds that of the osmium complex by a factor 4−5.

3. Anisotropy Amplitudes. Equation 7 provides the framework for a quantitative modeling of the polarization anisotropy data. This analysis shows that $r(t)$ is not only consistent with ILET, but further suggests the presence of a partially *delocalized* excited state at the instant of photoexcitation. These conclusions are based upon an examination of the anisotropy amplitudes associated with the excited-state absorption at early pump−probe delay times.

In the previous section it was established that the excited-state anisotropy decay is biphasic with fast and slow components arising from ILET and rotational diffusion, respectively. In the limit that no other transitions contribute to the excited-state absorption, the absorption anisotropy, $\langle r_\alpha(t)\rangle$, must have the following form:

$$\langle r_\alpha(t)\rangle = a_F^\lambda \exp(-k_F t) + a_S^\lambda \exp(-k_S t) \tag{9}$$

The time constants (k_F and k_S) are associated with the fast and slow decays of the anisotropy, respectively. The corresponding amplitudes (a_F^λ and a_S^λ) are both equal to −0.1 if photoexcitation promotes the electron to the ligand that lies along the polarization vector of the laser (i.e., creates a localized electronic state) and then, through ILET, scrambles among the three ligands. According to eq 7, the absorption anisotropy, $\langle r_\alpha(t)\rangle$, is only one of four contributions to $r(t)$. Thus, to obtain estimates of a_F^λ and a_S^λ, a quantitative modeling of the anisotropy data is required.

Details. The absorption and bleach contributions, α^T and β^T, are treated as input into the model and are determined from the magic angle data (A_{MA}) and ground-state absorption spectrum (A_{GS}). The bleach arises from the hole in the ground-state population, and thus its contribution should (1) appear instantaneously, (2) have a spectral shape that mirrors A_{GS}, and (3) be independent of pump−probe delay. This assumes that the bleach can only decay in amplitude via replenishment of the ground-state population. While this suggests a spectral shape for β^T it says nothing about its magnitude relative to α^T. Thus, to make progress the relative intensity of α^T and β^T (denoted by γ) must be known at a single (reference) wavelength, λ_{rt}, i.e., $\gamma_r = \alpha^T(\lambda_r)/\beta^T(\lambda_r)$. The absorption and bleach contributions are given in terms of A_{MA}, A_{GS}, and γ_r, by

$$\beta^T(\lambda) = \frac{3A_{MA}(\lambda_r)}{\gamma_r - 1}\left(\frac{A_{GS}(\lambda)}{A_{GS}(\lambda_r)}\right) \tag{10}$$

and

$$\alpha^T(\lambda,t) = 3A_{MA}(\lambda,t) + \beta^T(\lambda) \tag{11}$$

where t is the pump−probe delay. Thus, α^T and β^T are determined uniquely, provided that there is an independent measurement of γ_r. On the basis of known spectroscopic data[45,46] we estimate that at 370 nm γ_r is in the neighborhood of 1.8−2.4. By incorporating the magic angle data into the analysis, we account for the changes in the transient absorption signal intensity with pump−probe delay.

The final quantity needed for the anisotropy analysis is $\langle r_\beta(t)\rangle$. Because the bleach arises from the hole in the ground-state population, its anisotropy decays only through the rotational diffusion of the unexcited complexes. To the extent that the ground and excited states have the same rotational diffusion times, the bleach anisotropy takes on a particularly simple form:

$$\langle r_\beta(t)\rangle = r_{\beta 0}^\lambda \exp(-k_S t) \tag{12}$$

where $r_{\beta 0}^\lambda$ is the limiting value of the bleach anisotropy at a particular probe wavelength. We do not have direct experimental evidence from which to calculate an exact value of $r_{\beta 0}^\lambda$, as there is no definitive assignment of the ground-state absorption

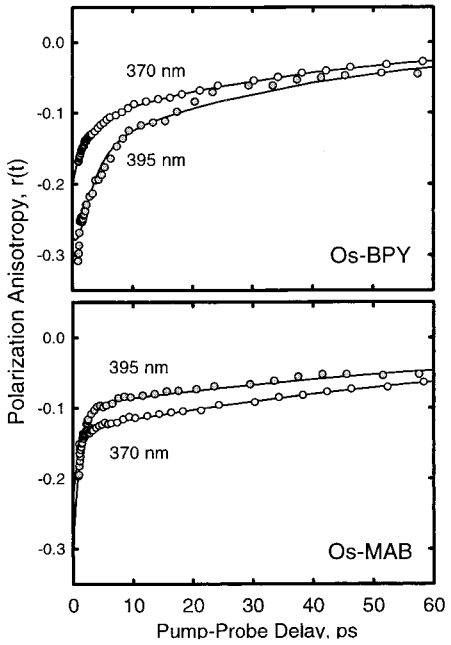

Figure 14. Comparison of experimental data and results of nonlinear least-squares fit to eq 7 as described in the text. The upper panel is for Os−BPY and lower panel is for Os−MAB. The regression involved the simultaneous fit to seven different probe wavelengths, but only two are shown in the figure for clarity.

band near 370 nm. The absorption spectrum is most likely a superposition of transitions that could be ligand-centered, metal-centered, or charge-transfer in nature, and $r_{\beta 0}^{\lambda}$ would be the weighted average of the limiting anisotropies for each transition. Thus, in our analysis, $r_{\beta 0}^{\lambda}$ is treated as an adjustable parameter that must take on a value in the range between −0.2 and +0.4. To simplify the model, we take $r_{\beta 0}^{\lambda}$ to be independent of probe wavelength, i.e., $r_{\beta 0}^{\lambda} \equiv r_{\beta 0}$. While this is probably not entirely correct, over a small spectral range it is a reasonable approximation. The treatment of $r_{\beta 0}$ as an adjustable parameter complicates matters, however, as there is a high correlation between it and a_S^{λ}. Thus, we are forced to examine the results of our analysis for different choices of $r_{\beta 0}$, eliminating those that yield physically unreasonable results. The criterion for excluding some values of $r_{\beta 0}$ is described in more detail below.

Analysis of Os−BPY Anisotropy. We first examined the polarization anisotropy data for Os−BPY. The anisotropy transients at seven probe wavelengths between 360 and 395 nm were simultaneously fit to the model described above. Rather than assign a_F^{λ} and a_S^{λ} exact values, in our analysis we treated both as adjustable parameters that can take on different values at each probe wavelength. For a given γ_r and $r_{\beta 0}$, the concurrent fit of seven transients requires 18 parameters—the excited-state anisotropy amplitudes, a_F^{λ} and a_S^{λ}, at each probe wavelength, and the two decay rates, k_F and k_S. A comparison between the fit to this model and the experimental data for Os−BPY is shown in the top panel of Figure 14. While seven transients were used in the analysis, only the transients at 370 and 395 nm are displayed for clarity. This fit was obtained with $\gamma_r = 2.1$ and $r_{\beta 0} = -0.09$.

Our primary interest is in the values obtained for a_F^{λ} and a_S^{λ}, the anisotropy amplitudes for the excited-state absorption. These are displayed for Os−BPY as the individual points in the upper panel of Figure 15. If the excited-state absorption arises from a single transition (or group of transitions with similar absorption characteristics), then $\langle r_\alpha(t) \rangle$ should be the same at all probe wavelengths throughout the absorption band. As demonstrated

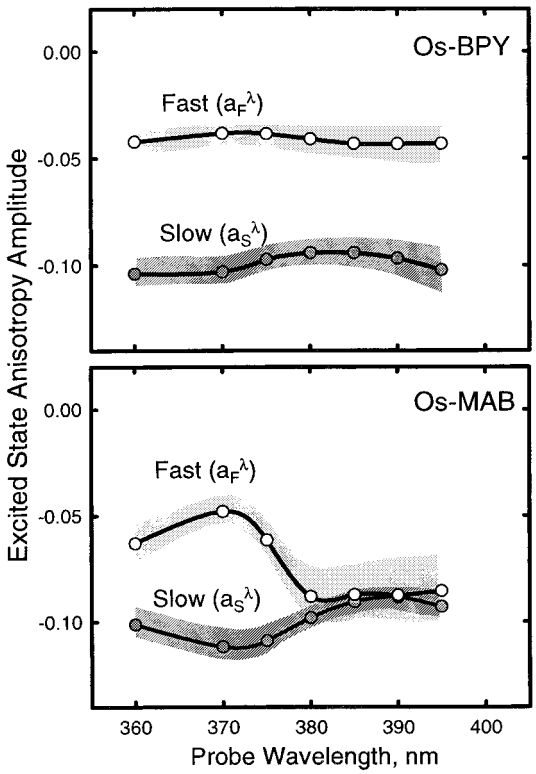

Figure 15. Excited-state anisotropy amplitudes (a_F^{λ} and a_S^{λ} from eq 9) displayed as a function of probe wavelength for Os−BPY (top panel) and Os−MAB (bottom panel). The two sets of points in each panel correspond to the anisotropy amplitudes on the fast and slow decay components. The individual points are obtained with $r_{\beta 0} = -0.09$ and $\gamma_r = 2.1$ (see text for details). The shaded areas illustrate the sensitivity of the analysis to these parameters as discussed in the text.

in the figure, the agreement between different probe wavelengths is reasonably good for both the fast and slow component amplitudes. Not all $r_{\beta 0}$ values yield the same degree of probe wavelength agreement, however, and we use this to eliminate some values of $r_{\beta 0}$. Choosing a different value for $r_{\beta 0}$ has little impact on the amplitude of the fast component (a_F^{λ}), but does influence the results for a_S^{λ}. The examination of a range of $r_{\beta 0}$ values shows that good probe wavelength agreement between the a_S^{λ} values is obtained only for $r_{\beta 0}$ between −0.11 and −0.08, with the best agreement being observed when $r_{\beta 0} = -0.09$. We have also examined the affect that varying γ_r has on the fit results. In contrast to $r_{\beta 0}$, using different values for γ_r only influences a_F^{λ}, the amplitude of the fast component. The sensitivity of this model to the choice of γ_r and $r_{\beta 0}$ is represented by the shaded areas in Figure 15, which correspond to the range of a_F^{λ} and a_S^{λ} values obtained when γ_r is in the range 1.8 to 2.4 and $r_{\beta 0}$ is between −0.11 and −0.08.

The excited-state anisotropy amplitudes obtained from this model are consistent with ILET. The amplitude of the slow component is ≈ −0.1, which is the value that is expected once the photoexcited electron randomizes among the three ligands. The initial anisotropy ($a_F^{\lambda} + a_S^{\lambda}$) is only −0.145. The initial anisotropy for a localized excitation is −0.2, provided that the excited-state absorption is dominated by the bpy^- absorption. In this limit, an initial anisotropy of −0.145 would imply that at the earliest pump−probe delay that can be measured with our apparatus (500 fs) only 63% of the initial population is on the photoselected ligand. This could be evidence for a rapid ILET process that occurs on a time scale that is not resolved in these experiments (<300−500 fs). The mechanism that would lead to such a fast delocalization is not at the moment clear. A

second possibility is that the photoexcitation of the ground-state ensemble produces a mixture of localized and delocalized excited states that arises from a distribution of local solvent environments. The purely localized states would have fast components (a_F^{λ}) equal to -0.1, while for purely delocalized states these would be equal to zero. Because the observed anisotropy is an ensemble average over all the solvent configurations present in the sample, the presence of a reduced anisotropy would imply that in a sizable fraction of the complexes, optical excitation prepares an excited-state wave function that is either delocalized (or partially delocalized) over at least two ligands.

Analysis of Os−MAB Anisotropy. The fit to the Os−MAB data is carried out using the same values for γ_r and $r_{\beta 0}$ that were used in the Os−BPY analysis. The comparison between the fit results and the experimental data is displayed in the lower panel of Figure 14, and the anisotropy amplitudes for the mixed ligand complex are shown in the lower panel of Figure 15. Like Os−BPY, the amplitude of the slow component is approximately -0.1 for all the probe wavelengths in this spectral region. Unlike Os−BPY, however, the amplitude of the fast component does depend on probe wavelength. To the red of 380 nm, where *mab* is the dominant absorber, the amplitude of this component is approximately -0.1; and to the blue of 380 nm, where *bpy* is the dominant absorber, it is around -0.05. This suggests that in the mixed-ligand complex there are two different electronic states produced by optical excitation—one that is localized on the unique ligand (in this case *mab*), and one that is partially delocalized over the other two. As in Os−BPY, this partially delocalized state is probably an ensemble average of localized and delocalized states arising from a distribution of local solvent environments. We must point out, however, that in the Os−MAB complex the time scale for the fast component is such that the amplitude analysis is a bit of an extrapolation. This introduces some uncertainty into the results and thus more experimentation is needed before a definitive conclusion can be reached.

E. Estimation of Ligand−Ligand Electronic Coupling. Taken together, the fast ILET rates and the observation of partial delocalization in the optically prepared electronic state suggests the presence of a large electronic coupling between the ligands. In this section we estimate a value for this coupling based on the driving force dependence of the ILET rate constants measured for the two complexes.

According to electron transfer theory,[54−58] the rate constant for electron transfer is determined by the activation energy (ΔG^*), the electronic coupling (H_{el}), and the solvent reorganization energy (λ). The most common formalisms treat electron transfer in either the adiabatic or the nonadiabatic regime. Rips and Jortner[57,58] extended the theory to include the solvent reorganization time (τ_s) and thereby bridge the two limits, i.e.,

$$k_{ET} = \left(\frac{1}{1+\kappa}\right)\frac{H_{el}^2}{\hbar}\sqrt{\frac{\pi}{\lambda k_B T}}\exp(-\Delta G^*/k_B T) \qquad (13)$$

where the quantity κ, known as the adiabaticity parameter, is given by

$$\kappa = \frac{4\pi H_{el}^2 \tau_s}{\hbar\lambda} \qquad (14)$$

As the electronic coupling increases, the activation energy (ΔG^*) is no longer related to the driving force (ΔG_o) by $\Delta G^* = (\lambda + \Delta G_o)^2/4\lambda$. Brunschwig and Sutin[59] developed an expression for the activation energy in the limit of large H_{el}, i.e.,

$$\Delta G^* = \frac{\lambda}{4} + \frac{\Delta G_o}{2} + \frac{(\Delta G_o)^2}{4(\lambda - 2H_{el})} - H_{el} + \frac{H_{el}^2}{\lambda + \Delta G_o} \qquad (15)$$

Together, eqs 13, 14, and 15 describe the electron-transfer rate constant for electronic couplings that span the adiabatic and nonadiabatic limits. Electron-transfer reactions that take place in the conventional nonadiabatic limit have $\kappa \ll 1$ and the well-known expression for the electron-transfer rate constant is recovered.[57] For electron-transfer reactions in the adiabatic limit, where $\kappa \gg 1$, the preexponential factor scales with the inverse of the solvent reorganization time, $1/\tau_s$. We have modeled our ILET data using these equations, and for the analysis we need estimates of both the reorganization time (τ_s) and reorganization energy (λ).

Solvent reorganization times have been measured for a number of solvents. These experiments show that typically there is more than one time scale associated with solvent motion, even in simple solvents. Acetonitrile exhibits two characteristic time scales: fast "inertial" motion (sub-100 fs) and slower "diffusive" motion (2−3 ps).[51] In our analysis we use an *average* reorganization time of 0.5 ps. An estimate of the reorganization energy can be obtained from dielectric continuum theory. Brunschwig and Sutin[60] developed a general expression for the outer-sphere reorganization energy arising from the redistribution of charge within a spherical cavity. For the case of interligand electron hopping, the outer-sphere contribution to λ is given by

$$\lambda = \frac{1}{2a}\left[\left(\frac{1}{D_{in}} - \frac{1}{D_S}\right)\sum_{n=1}^{\infty} g_n(\Delta e)\left(1 + \left(\frac{n}{n+1}\right)\frac{D_{in}}{D_S}\right)^{-1} - \left(\frac{1}{D_{in}} - \frac{1}{D_{OP}}\right)\sum_{n=1}^{\infty} g_n(\Delta e)\left(1 + \left(\frac{n}{n+1}\right)\frac{D_{in}}{D_{OP}}\right)^{-1}\right] \qquad (16)$$

where D_{in}, is the dielectric constant inside the cavity (usually taken to be unity), D_S and D_{OP} are the static and optical dielectric constants, and $g(\Delta e)$ is

$$g_n(\Delta e) = 2(\Delta e)^2\left(\frac{r}{R}\right)^{2n}[1 - P_n(\cos(\theta))] \qquad (17)$$

Here r is the distance of the photoexcited electron from the metal center, R is the radius of the cavity, and θ is the angle between the ligands (120°). On the basis of reasonable estimates for each of these parameters, we estimate outer-sphere contribution to λ to be in the range of 2000−3500 cm^{-1}. The Meyer group[61] has observed a broad absorption band in the MLCT excited state near 4700 cm^{-1}. This band could be the result of a ligand-to-ligand optical excitation, and could thus yield a direct measure of the reorganization energy.

For a given choice of λ, we can estimate H_{el} using eqs 13−15. Shown in Figure 16 are the ILET rate constants for Os−BPY and Os−MAB as a function of the electron-transfer driving force. The solid line is calculated from these equations using λ = 3500 cm^{-1}, τ_s = 0.5 ps, and H_{el} = 570 cm^{-1}. We have explored a range of values for λ in a similar manner. When λ is between 1800 and 4700 cm^{-1}, our analysis suggests that H_{el} is between 200 and 900 cm^{-1}. In all cases, the adiabaticity parameter, κ, is much greater than 1, suggesting that ILET takes place in the adiabatic limit.

IV. Conclusions

We have used femtosecond polarization anisotropy methods to investigate the interligand electron transfer (ILET) dynamics

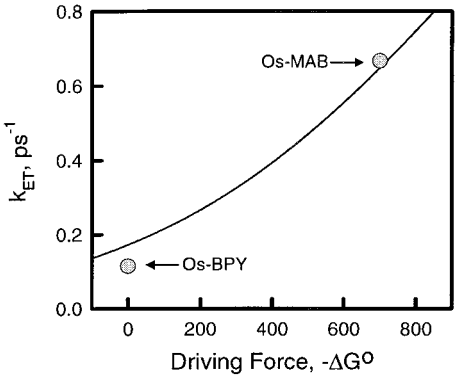

Figure 16. Electron-transfer rate constant as function of driving force. Points are experimental observation for Os−BPY and Os−MAB. The line is calculated from eq 14−16 with $\lambda = 3500$ cm^{-1} and $H_{el} = 570$ cm^{-1}.

in Os−BPY and one of its mixed-ligand analogues, Os−MAB. Our data show that ILET in Os−BPY has a rate constant of $(8.1\ \text{ps})^{-1}$, much faster than previously thought. There is a driving force for ILET in the Os−MAB complex that increases the ILET rate constant to $(1.5\ \text{ps})^{-1}$. Examination of the ILET process in different solvents shows that the ILET time scales with the solvent reorganization time, implying that electron transfer occurs in the strongly coupled (adiabatic) limit. An analysis of the anisotropy amplitudes suggests that a substantial portion of the excited-state ensemble is created with delocalized (or partially delocalized) excited-state wave functions.

Acknowledgment. Funding for this project was provided by The University of North Carolina at Chapel Hill and The Research Corporation (RI0048). We also thank T. J. Meyer for a number of stimulating discussions.

References and Notes

(1) Meyer, T. J. *Pure Appl. Chem.* **1986**, *50*, 1293.
(2) Casper, J. V.; Meyer, T. J. *J. Am. Chem. Soc.* **1983**, *105*, 5583.
(3) Casper, J. V.; Kober, E. M.; Sullivan, B. P.; Meyer, T. J. *J. Am. Chem. Soc.* **1982**, *104*, 630.
(4) Van Houten, J.; Watts, R. J. *J. Am. Chem. Soc.* **1976**, *98*, 4853.
(5) Van Houten, J.; Watts, R. J. *Inorg. Chem.* **1978**, *17*, 3381.
(6) Bradley, P. G.; Kress, N.; Hornberger, B. A.; Dallinger, R. F.; Woodruff, W. H. *J. Am. Chem. Soc.* **1981**, *103* (25), 7441−7446.
(7) Mabrouk, P. A.; Wrighton, M. S. *Inorg. Chem.* **1986**, *25* (4), 526−531.
(8) Vlcek, A. *Coord. Chem. Rev.* **2000**, *200*−*202*, 933−977.
(9) Ferguson, J.; Herren, F.; Krausz, E.; Maeder, M.; Vrbancich, J. *Coord. Chem. Rev.* **1985**, *64*, 21.
(10) Ferguson, J.; Herren, F. *Chem. Phys.* **1983**, *76*, 45−59.
(11) Creutz, C.; Chou, M.; Netzel, T. L.; Okumura, M.; Sutin, N. *J. Am. Chem. Soc.* **1980**, *102* (4), 1309−1319.
(12) Damrauer, N. H.; Cerullo G.; Yeh, A.; Boussie, T. R.; Shank, C. V.; McCusker, J. K. *Science* **1997**, *275*, 54−57.
(13) Damrauer, N. H.; McCusker, J. K. *J. Phys. Chem. A* **1999**, *103* (42), 8440−8446.
(14) Yeh, A. T.; Shank, C. V.; McCusker, J. K. *Science* **2000**, *289*, 935−938.
(15) Cushing, J. P.; Butoi, C.; Kelley, D. F. *J. Phys. Chem. A* **1997**, *101* (39), 7222−7230.
(16) Pogge, J. L.; Kelley, D. F. *Chem. Phys. Lett.* **1995**, *238*, 16−24.
(17) Malone, R. A.; Kelley, D. F. *J. Chem. Phys.* **1991**, *95* (12), 8970−8976.
(18) Cooley, L. F.; Bergquist, P.; Kelley, D. F. *J. Am. Chem. Soc.* **1990**, *112*, 2612−2617.
(19) Yabe, T.; Orman, L. K.; Anderson, D. R.; Yu, S.-C.; Xu, X.; Hopkins, J. B. *J. Phys. Chem.* **1990**, *94* (18), 7128−7132.
(20) Chang, Y. J.; Xu, X.; Yabe, T.; Yu, S.-C.; Anderson, D. R.; Orman, L. K.; Hopkins, J. B. *J. Phys. Chem.* **1990**, *94* (2), 729−736.
(21) Carroll, P. J.; Brus, L. E. *J. Am. Chem. Soc.* **1987**, *109*, 7613−7616.
(22) Carlin, C. M.; DeArmond, M. K. *J. Am. Chem. Soc.* **1985**, *107*, 53−57.
(23) Önfelt, B.; Lincoln, P.; Nordén, B.; Baskin, J. S.; Zewail, A. H. *Proc. Natl. Acad. Sci. U.S.A.* **2000**, *97* (11), 5708−5713.
(24) Liard, D. J.; Vlcek, A. *Inorg. Chem.* **2000**, *39* (3), 485−490.
(25) Hagfeldt, A.; Grätzel, M. *Chem. Rev.* **1995**, *95*, 49−68.
(26) Bignozzi C. A.; Schoonover, J. R.; Scandola, F. *Prog. Inorg. Chem.* **1997**, *44*, 1−95.
(27) Balzani, V.; Credi, A.; Scandola, F. *Transition Metals in Supramolecuar Chemistry*; Fabbrizzi, L., Poggi, A., Eds.; Kluwer: The Netherlands, 1994; p 1.
(28) Fleming, C. N.; Maxwell, K. A.; Meyer, T. J.; Papanikolas, J. M. *J. Am. Chem. Soc.* **2001**, *123* (42), 10336−10347.
(29) Smith, G. D.; Maxwell, K. A.; Desimone, J. M.; Meyer, T. J.; Palmer, R. A. *Inorg. Chem.* **2000**, *39* (5), 893−898.
(30) Maxwell, K. A. Doctoral Dissertation, University of North Carolina at Chapel Hill, Chapel Hill, NC, 1999.
(31) Kober, E. M.; Sullivan, B. P.; Meyer, T. J. *Inorg. Chem.* **1984**, *23* (14), 2098−2104.
(32) Riesen, H.; Wallace, L.; Krausz, E. *Inorg. Chem.* **2000**, *39*, 5044−5052.
(33) Riesen, H.; Krausz, E. *Chem. Phys. Lett.* **1998**, *287*, 388−394.
(34) Karka, L.; Hupp, J. T. *Inorg. Chem.* **1997**, *36* (15), 3318−3321.
(35) Oh, D. H.; Boxer, S. G. *J. Am. Chem. Soc.* **1989**, *111*, 1131−1133.
(36) Yersin, H.; Strasser, J. *Coord. Chem. Rev.* **2000**, *208*, 331−364.
(37) Yersin, H.; Humbs, W. *Inorg. Chem.* **1999**, *38*, 5820−5831.
(38) Humbs, W.; Strasser, J.; Yersin, H. *J. Lumin.* **1997**, *72*−*74*, 677−678.
(39) Huber, P.; Yersin, H. *J. Phys. Chem.* **1993**, *97* (49), 12705−12709.
(40) Riesen, H.; Wallace, L.; Krausz, E. *J. Chem. Phys.* **1995**, *102* (12), 4823.
(41) Demas, J. N.; Crosby, G. A. *J. Phys. Chem.* **1971**, *75*, 991.
(42) Demas, J. N.; Crosby, G. A. *J. Am. Chem. Soc.* **1971**, *93*, 2841.
(43) Kober, E. M.; Meyer, T. J. *Inorg. Chem.* **1984**, *23*, 3877−3886.
(44) Lumpkin, R. S.; Kober, E. M.; Worl, L. A.; Murtaza, Z.; Meyer, T. J. *J. Phys. Chem.* **1990**, *94*, 239−243.
(45) Noble, B.; Peacock, R. D. *Inorg. Chem.* **1996**, *35* (6), 1616−1620.
(46) Noble, B.; Peacock, R. D. *Spectrochim. Acta, Part A* **1990**, *46* (3), 407−412.
(47) Braterman, P. S.; Harriman, A.; Heath, G. A.; Yellowlees, L. J. *J. Chem. Soc., Dalton Trans.* **1983**, 1801−1803.
(48) Heath, G. A.; Yellowlees, L. J.; Braterman, P. S. *Chem. Commun.* **1981**, 287−289.
(49) Konig, E.; Kremer, S. *Chem. Phys. Lett.* **1970**, *5*, 87.
(50) Decurtins, S.; Felix, F.; Ferguson, J.; Güdel, H. U.; Ludi, A. *J. Am. Chem. Soc.* **1980**, *102* (12), 4102−4107.
(51) Passino, S. A.; Nagasawa, Y.; Fleming, G. R. *J. Chem. Phys.* **1997**, *107* (16), 6094−6108.
(52) Jonas, D. M.; Lang, M. J.; Nagasawa, Y.; Joo, T.; Fleming, G. R. *J. Phys. Chem.* **1996**, *100*, 12660−12673.
(53) Martinsson, P.; Oksanen, J. A. I.; Hilgendorff, M.; Hynninen, P. H.; Sundstrom, V.; Akesson, E. *Chem. Phys. Lett.* **1999**, *309* (5−6), 386−394.
(54) Sutin, N. *Adv. Chem. Phys.* **1999**, *106*, 7−33.
(55) Newton, M. D.; Sutin, N. *Annu. Rev. Phys. Chem.* **1984**, *35*, 437−480.
(56) Barbara, P. F.; Meyer, T. J.; Ratner, M. A. *J. Phys. Chem.* **1996**, *100* (31), 13148−13168.
(57) Rips, I.; Jortner, J. *J. Chem. Phys.* **1987**, *87* (4), 2090−2105.
(58) Rips, I.; Jortner, J. *J. Chem. Phys.* **1987**, *87* (11), 6513−6519.
(59) Brunschwig, B. S.; Sutin, N. *Coord. Chem. Rev.* **1999**, *187*, 233−254.
(60) Brunschwig, B. S.; Ehrenson, S.; Sutin, N. *J. Phys. Chem.* **1987**, *91*, 1 (18), 4714−4723.
(61) Meyer, T. J. Personal communication.